Analytica Chimica Acta 758 (2013) 66–71

Contents lists available at SciVerse ScienceDirect

Analytica Chimica Acta

journal homepage: www.elsevier.com/locate/aca

A novel amperometric biosensor for superoxide anion based on superoxide dismutase immobilized on gold nanoparticle-chitosan-ionic liquid biocomposite film

Lu Wang, Wei Wen, Huayu Xiong, Xiuhua Zhang, Haoshuang Gu, Shengfu Wang*

Ministry of Education Key Laboratory for the Synthesis and Application of Organic Functional Molecules & College of Chemistry and Chemical Engineering, Hubei University, Wuhan 430062, PR China

HIGHLIGHTS

- SOD was immobilized in gold nanoparticles-chitosan-ionic liquid (GNPs-CS-IL) film.
- The biosensor was constructed by one-step ultrasonic electrodeposition of GNPs-CS-IL onto GCE.
- The biosensor showed excellent analytical performance for $O_2^{\bullet -}$ real-time analysis.

GRAPHICAL ABSTRACT

Schematic representation of the assembly process of SOD/GNPs-CS-IL/GCE.

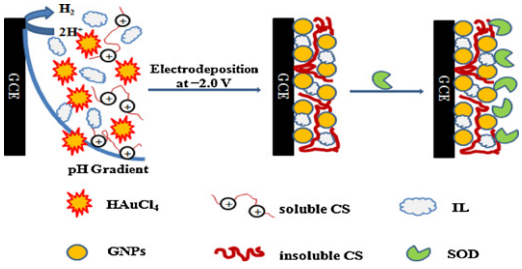

ARTICLE INFO

Article history:
Received 9 August 2012
Received in revised form 23 October 2012
Accepted 26 October 2012
Available online 9 November 2012

Keywords:
Superoxide anion
Superoxide dismutase
Gold nanoparticles
Ionic liquid
Ultrasonic electrodeposition

ABSTRACT

A novel superoxide anion ($O_2^{\bullet -}$) biosensor is proposed based on the immobilization of copper-zinc superoxide dismutase (SOD) in a gold nanoparticle-chitosan-ionic liquid (GNPs-CS-IL) biocomposite film. The SOD-based biosensor was constructed by one-step ultrasonic electrodeposition of GNP-CS-IL composite onto glassy carbon electrode (GCE), followed by immobilization of SOD on the modified electrode. Surface morphologies of a set of representative films were characterized by scanning electron microscopy. The electrochemical performance of the biosensor was evaluated by cyclic voltammetry and chronoamperometry. A pair of quasi-reversible redox peaks of SOD with a formal potential of 0.257 V was observed at SOD/GNPs-CS-IL/GCE in phosphate buffer solution (PBS, 0.1 M, pH 7.0). The effects of varying test conditions on the electrochemical behavior of the biosensor were investigated. Furthermore, several electrochemical parameters were calculated in detail. Based on the biomolecule recognition of the specific reactivity of SOD toward $O_2^{\bullet -}$, the developed biosensor exhibited a fast amperometric response (<5 s), wide linear range (5.6–2.7 × 10^3 nM), low detection limit (1.7 nM), and excellent selectivity for the real-time measurement of $O_2^{\bullet -}$. The proposed method is promising for estimating quantitatively the dynamic changes of $O_2^{\bullet -}$ in biological systems.

1. Introduction

The superoxide anion ($O_2^{\bullet -}$), the primary species of reactive oxygen species (ROS), is closely implicated in many physiological and pathological processes [1]. On the one hand, it functions as a defense against viral or bacterial attack. On the other hand, it can lead to damage of proteins, DNA, and lipid structures in the human body [2]. The excessive generation of $O_2^{\bullet -}$ may induce

Abbreviations: $O_2^{\bullet -}$, superoxide anion; SOD, superoxide dismutase; GNPs-CS-IL, gold nanoparticle-chitosan-ionic liquid; GCE, glassy carbon electrode; ROS, reactive oxygen species; GNPs, gold nanoparticles; CS, chitosan; IL, ionic liquid; XOD, xanthine oxidase; XAN, xanthine; [bmim][BF_4], 1-butyl-3-methylimidazolium tetrafluoroborate; CV, cyclic voltammetry; $E^{0\prime}$, formal potential; E_{pa}, peak potential; E_{pc}, cathodic peak potential; E_p, peak-to-peak separation; AA, ascorbic acid; UA, uric acid.

* Corresponding author. Tel.: +86 27 50865309; fax: +86 27 88663043.
E-mail address: wangsf@hubu.edu.cn (S. Wang).

0003-2670/$ – see front matter © 2012 Elsevier B.V. All rights reserved.
http://dx.doi.org/10.1016/j.aca.2012.10.050

pathological conditions including cancer, stoke, and progressive neurodegenerative disease [3]. Hence, evaluating dynamic changes in the superoxide concentration quantitatively is of great significance in a variety of in vitro and in vivo models. However, it is a long-standing and relatively challenging problem because of the high reactivity, short half-life (in the ms to s range), and rather low basal concentration of $O_2^{\bullet -}$ in a biological system [2]. To date, extensive efforts have been devoted to assaying $O_2^{\bullet -}$, by methods including electron spin resonance (ESR) [4], high performance liquid chromatography, triple quadrupole mass spectrometry [5], and chemiluminesence [6]. A majority of these methods suffered from serious limitations, however. For instance, although ESR can detect free radicals directly, it is limited by its low sensitivity and the cost of ESR spectrometers [7]. Nowadays, the electrochemical method appears much more attractive for determining $O_2^{\bullet -}$, mainly due to its advantages of high sensitivity and good selectivity, and its capability in terms of direct and real-time detection [8]. Of the hitherto-reported approaches to the electrochemical measurement of $O_2^{\bullet -}$, the enzyme sensor has attracted a great deal of interest over the past several years.

It is well recognized that (copper, zinc)-superoxide dismutase (SOD), ubiquitously distributed in aerobic organisms, can protect organisms from the toxic effects of $O_2^{\bullet -}$ by specifically catalyzing the dismutation of $O_2^{\bullet -}$ to O_2 and H_2O_2. So, electrochemical studies of SOD are very necessary to understand the intrinsic thermodynamic and kinetic properties of SOD and to prepare SOD-based third-generation biosensors for $O_2^{\bullet -}$ [2,9]. Recently, several strategies have been employed to realize direct electron transfer of SOD, for example, the use of nanomaterials [9,10]. Gold nanoparticles (GNPs) have been widely used to immobilize enzymes because of their large surface area and their good biocompatibility and conductivity [11,12]. One approach for the preparation of GNPs is electrodeposition, which allows control of the particle size and distribution of GNPs by varying the deposition potential, concentration, buffer solution, and deposition time [10]. In particular, ultrasonic electrodeposition combines the features of ultrasound and electrodeposition, and thus exhibits good performance in fabricating well-dispersed GNPs [13]. Uncoated GNPs, however, are sensitive to environmental factors, such as pH, temperature, and solvents, because of the strong reactivity of the free electrons present on their surfaces [14]. So, they easily tend to aggregate when used in such media. To address this challenge, protective species, such as chitosan (CS), may be added to stabilize the GNPs [14].

CS is an aminopolysaccharide biopolymer, possessing many useful properties such as excellent film forming ability, biocompatibility, and high mechanical strength [15]. Consequently, the net charge and solubility of CS is pH-dependent. Usually, electrodeposition is carried out at reducing potential, and H^+ in solution is consumed at the cathode. Using the locally generated H^+ gradient, acidic side chains of CS are titrated. As a result, the solubility of CS is changed, leading to the controlled deposition of a CS film [16]. Furthermore, CS-based biocomposite films could be conveniently prepared by effective incorporation of functional substrates such as ionic liquids (ILs). ILs are ionic compounds composed of bulky asymmetric cations and small anions, which preserve their liquid state over a wide temperature range [17]. They have attracted much attention due to their low toxicity, wide potential window, high thermal stability, good conductivity, and electrochemical stability [18].

Herein, a novel $O_2^{\bullet -}$ biosensor was fabricated by immobilizing SOD on a one-step ultrasonically electrodeposited GNP-CS-IL film. In the electrodeposition process, a $HAuCl_4$ solution was first mixed with CS and IL, and then electrochemically reduced under a certain voltage. The produced GNPs were deposited onto glassy carbon electrode (GCE) along with IL-incorporated CS.

2. Experimental

2.1. Reagents and apparatus

Bovine erythrocyte copper-zinc superoxide dimutase (SOD), xanthine oxidase (XOD), and CS were bought from Sigma (USA). The concentration of SOD stock solution, prepared by directly dissolving SOD in 0.1 M phosphate buffer solution (PBS, pH 7.0), was 3000 U mL^{-1}. A 5 mg mL^{-1} CS aqueous solution was prepared by ultrasonically dissolving CS in 0.1 M acetic acid. Then, the pH of —CS solution was adjusted to 5.0 using 1.0 M NaOH. $HAuCl_4{\cdot}4H_2O$ (Au% > 48%) and xanthine (XAN) were provided by Aldrich. 1-Butyl-3-methylimidazolium tetrafluoroborate ([bmim][BF_4]), a hydrophilic IL, was purchased from Chengjie Chemical Ltd. Corp. (Shanghai, China). The supporting electrolyte solution for experiments was 0.1 M pH 7.0 PBS. All other chemicals were of analytical reagent grade. Deionized double-distilled water was used throughout the experiments.

All the electrochemical measurements were performed on a CHI 660A electrochemical workstation. A standard three-electrode system, with a film-modified GCE as working electrode, a saturated calomel electrode (SCE) as reference electrode, and platinum foil as auxiliary electrode, was used in the measurements. All potentials given in this paper are referred to SCE. Nitrogen atmosphere was maintained during the measurements. The pH value of the electrolyte was determined by a 320-S acidity meter (Mettler-Toledo, Switzerland). A JEOL JSM-5510LV scanning electron microscope (SEM, Japan) was applied for characterizing the prepared samples.

2.2. Preparation of biosensor

The preparation process for the biosensor is described in Scheme 1. The electrochemical deposition process was first carried out by dipping the pretreated GCE in a CS solution containing 0.2 mg mL^{-1} $HAuCl_4$ and 1% IL at −2.0 V for 300 s under ultrasonic irradiation. Then, the resulting electrode was removed from the solution and thoroughly rinsed with water. After drying, 5 μL SOD solution (3000 U mL^{-1}) was dropped onto GNP-CS-IL/GCE surface, and the electrode referred in the text as SOD/GNP-CS-IL/GCE was fabricated. For comparison, GNP-CS-IL/GCE, SOD/GNP-CS/GCE, and SOD/CS-IL/GCE were also prepared by analogous procedures.

3. Results and discussion

3.1. Morphology characterization of the fabricated biosensor

Morphologies of a set of typical films were explored by SEM (Fig. 1). The image of SOD film (Fig. 1a) contained bright globular shapes, which were attributed to the deposition of heavily aggregated SOD molecules. GNP-CS film (Fig. 1b) showed a large number of uniform granular protuberances. Such well-dispersed GNP-CS particles may be related to the effects of CS. It is reasonable to deduce that positively charged CS could bind $AuCl_4^-$, and that amine groups of CS could interact with GNPs [19]. The image of GNP-CS-IL showed that the nanoparticles had a quite uniform distribution (Fig. 1c). It is deduced that the application of IL block the aggregation of nanoparticles (NPs) to a certain extent. As shown in Fig. 1d, SOD/GNP-CS membrane looked rough and incompact, with some agglomerates, which indicated the aggregation of SOD. A rather uniform and smooth surface with orderly nanopores could be observed in SOD/GNP-CS-IL matrix (Fig. 1e), which may arise from the following aspects. IL has low interface tension and thus can enhance the nucleation rate, which helps the formation of smaller GNP-CS particles [20]. Additionally, IL might act as a template, like alkylammonium surfactants and amphiphilic block copolymers [21].

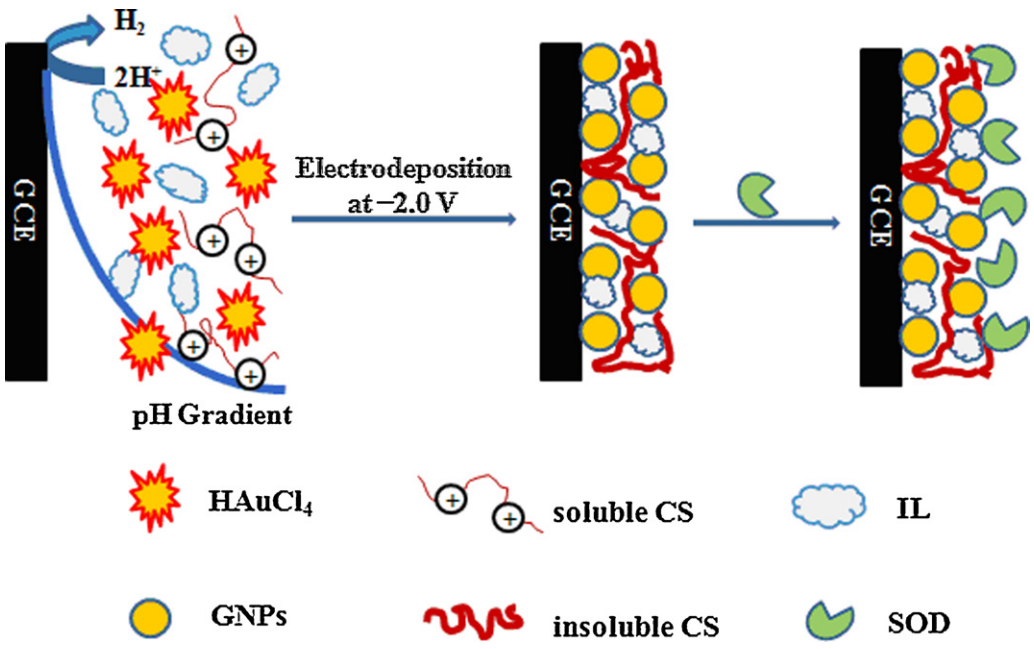

Scheme 1. Schematic representation of the assembly process of SOD/GNPs-CS-IL/GCE.

3.2. Cyclic voltammetry characterization of the biosensor

To discern the role of each component and the possible synergy between them, cyclic voltammograms (CVs) of different electrodes were collected and displayed in Fig. 2. No response was observed for GNP-CS-IL/GCE (Fig. 2a). A pair of quasi-reversible redox peaks with formal potential ($E^{0'}$) of 0.257 V appeared for SOD/GNP-CS-IL/GCE (Fig. 2b), suggesting that the pair of peaks resulted from the electrochemical redox reaction of the copper moiety in SOD [22]. Without IL, the current response of SOD/GNP-CS/GCE matrix (Fig. 2c) was faint and feeble, meaning that IL played an important role in facilitating the direct electron transfer of SOD. Without GNPs, peak currents decreased remarkably, and the cathodic peak became ill-defined in SOD/CS-IL/GCE (Fig. 2d), demonstrating that the GNPs significantly promoted the electron transfer between SOD and the electrode. Therefore, the integration of IL with GNPs was responsible for an extraordinary synergistic enhancement of the electron transfer rate of SOD. Moreover, the highly porous structure of SOD/GNP-CS-IL, produced due to the generation of H_2 bubbles during the electrodeposition process, had many positive effects, such as facilitating mass access, making substrate transport effective, releasing the inner stress of the film, and preventing phase

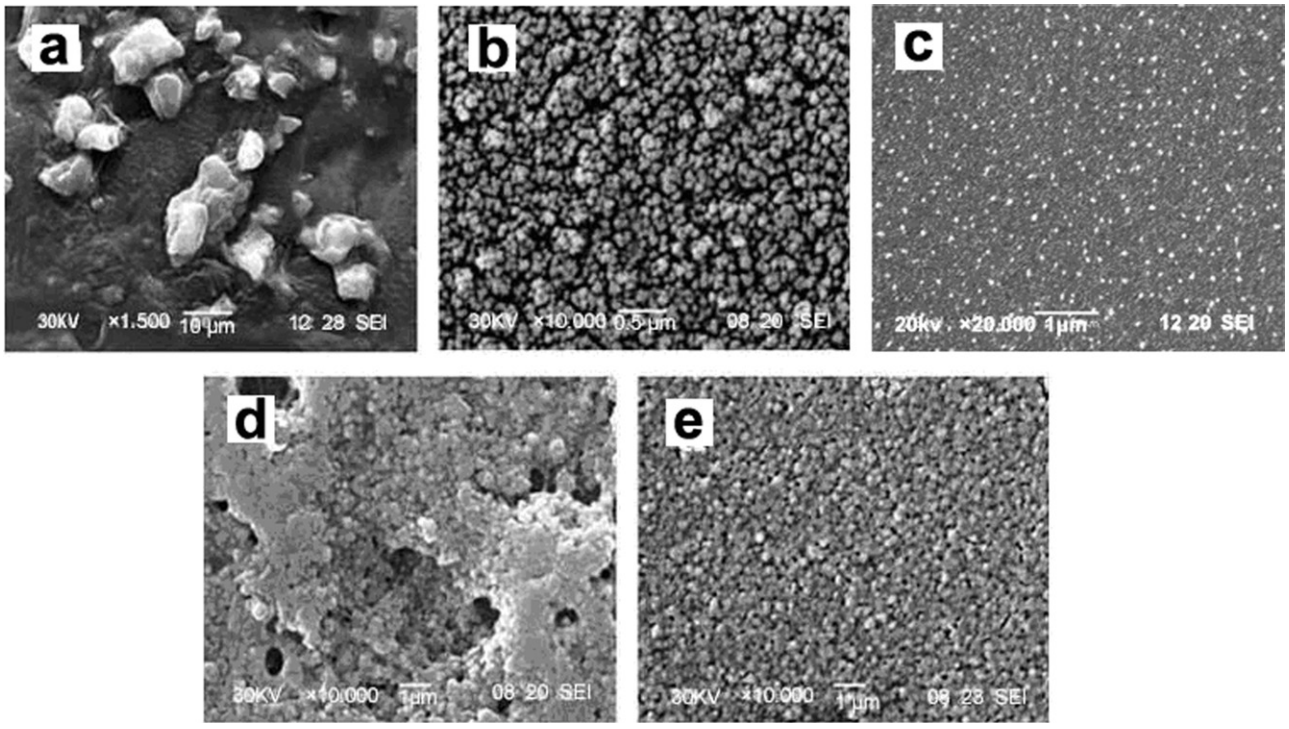

Fig. 1. SEM images of (a) SOD, (b) GNP-CS, (c) GNP-CS-IL, (d) SOD/GNP-CS, and (e) SOD/GNP-CS-IL on glassy carbon.

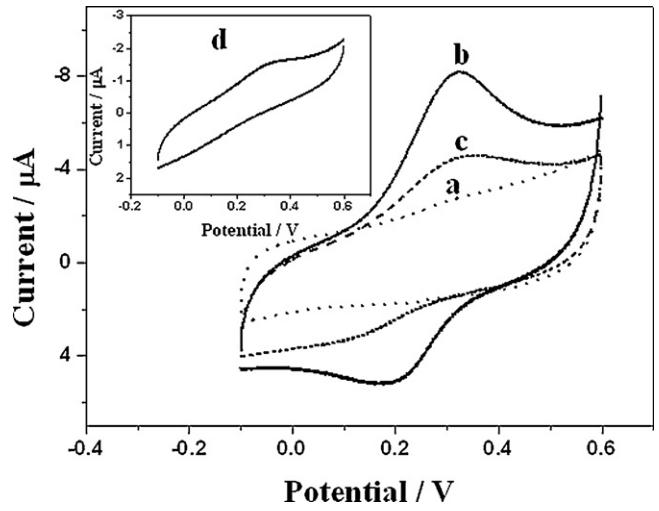

Fig. 2. CVs of (a) GNP-CS-IL/GCE, (b) SOD/GNP-CS-IL/GCE, (c) SOD/GNP-CS/GCE, and (d) SOD/CS-IL/GCE in 0.1 M pH 7.0 PBS at a scan rate of 0.1 V s^{-1}.

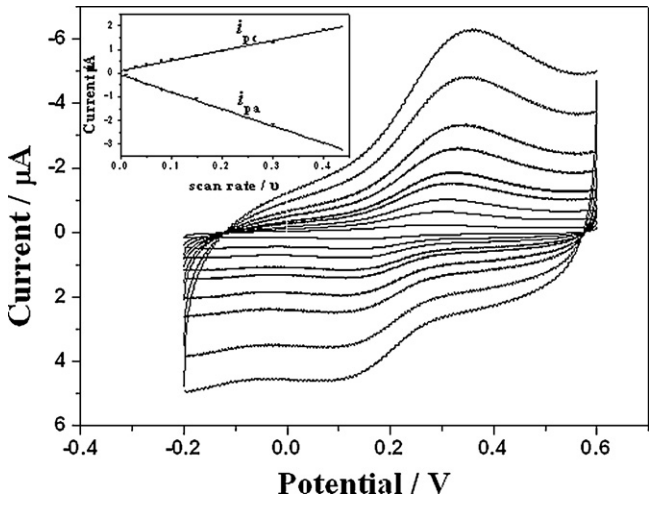

Fig. 4. CVs of SOD/GNP-CS-IL/GCE at different scan rates (from inner to outer): 10, 30, 50, 80, 100, 150, 200, 300, and 400 mV s^{-1} in 0.1 M pH 7.0 PBS. Inset: plots of peak currents vs. scan rate.

cracking [23]. All these had benefits for the good performance of the biosensor.

3.3. Selection of the optimum experimental conditions

3.3.1. Influence of pH on the electrochemical behaviors of the biosensor

The effects of the pH of the supporting electrolyte on the electrochemical behaviors of SOD were investigated over the range of 4.0–8.5. As shown in Fig. 3A, peak potentials shifted negatively with increasing pH, implying that the electrochemical process involved proton transfer. Furthermore, the anodic peak potential (E_{pa}), the cathodic peak potential (E_{pc}), and $E^{0\prime}$ were all linearly dependent on pH, with slope values of 40, 50, and 45 mV/pH, respectively. All those slope values are close to the theoretical value of 57.6 mV/pH at 18 °C [24], giving evidence that the electrode reaction of SOD is a one electron transfer accompanied by an equal number of protons. The cathodic peak currents changed significantly over the pH range (see Fig. 3B). The maximum value of the peak currents was achieved at pH 7.0. So, pH 7.0 was deemed to be the optimum pH and used in the further experiments.

3.3.2. Influence of scan rate on electrochemical behaviors of the biosensor

CVs of SOD/GNP-CS-IL/GCE with scan rates in the range from 10 to 400 mV s^{-1} were collected and shown in Fig. 4. With increasing scan rate, the anodic and cathodic peak currents of SOD increased continually, while the peak-to-peak separation (ΔE_p) also increased. The linear dependence of the anodic and cathodic peak currents on the scan rate (inset of Fig. 4) revealed that the electron transfer process of SOD was surface-confined. What is more, the charge consumed (Q), obtained by the integration of the reduction peaks, remained almost unchanged regardless of scan rate. According to Faraday's law [25], $Q = nFA\Gamma^*$ (where n is the number of electrons transferred, and F and A stand for the Faraday constant and the geometric area of the modified electrode surface, respectively). Therefore, Γ^* (surface coverage) of electro-active SOD in SOD/GNP-CS-IL/GCE was estimated to be the 4.55×10^{-10} mol cm^{-2}, which was about 4 times as large as the 1.04×10^{-10} mol cm^{-2} for SOD/GNP/ITO [10] and 7.3 times higher than the 6.2×10^{-11} mol cm^{-2} for SOD/nano-Au/GCE [26]. It was inferred that the favorable microenvironment, such as the nanometer dimensions and larger surface area provided by the well-dispersed GNP-CS-IL matrix contributed to the high load of electroactive SOD.

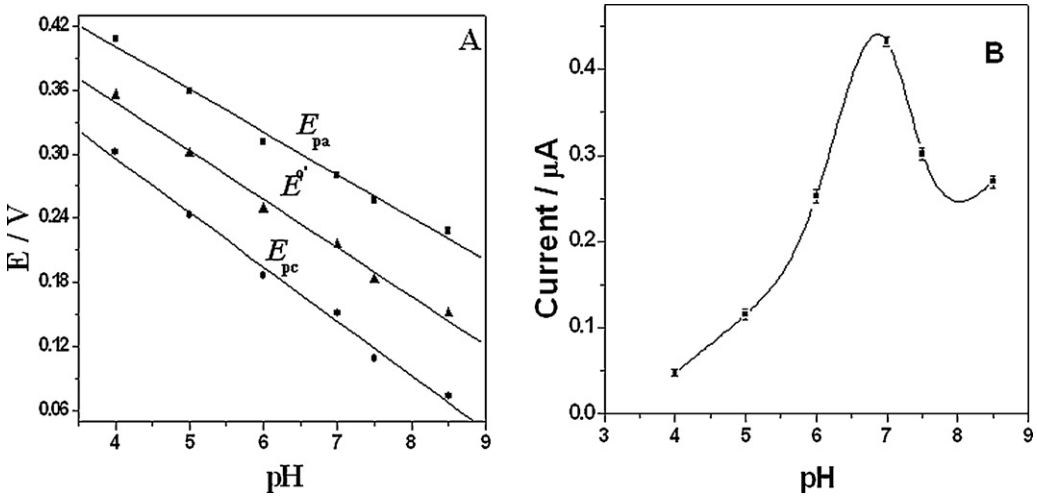

Fig. 3. (a) Plots of E_p vs. pH. (b) Influence of pH on cathodic peak current of SOD/GNP-CS-IL/GCE in 0.1 M PBS at a scan rate of 0.03 V s^{-1}.

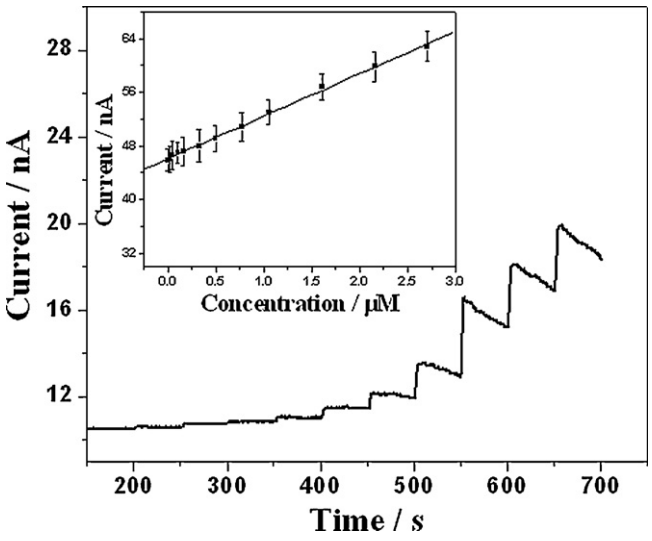

Fig. 5. Amperometric response of SOD/GNP-CS-IL/GCE upon successive XAN injection under stirring into 4 mL of 0.1 M pH 7.0 PBS containing 0.002 U mL^{-1} XOD. An applied potential of −0.15 V was chosen as a compromise between the highest response of the sensor to $O_2^{\bullet-}$ and the lowest current background. Inset: calibration curve for superoxide; the data points for the quantitative results were obtained 25 s later, after the addition of XAN to the solution.

Based on the Laviron theory [27] and the potential scan rate dependence of the anodic and cathodic peak potentials, the relevant kinetic parameters of electrode reaction, i.e., the electron transfer coefficient (α) and the heterogeneous electron transfer rate constant (k_s), were calculated to be 0.44 and 4.7 s^{-1}, respectively. The excellent electron transfer properties of SOD may be due to the synergetic action of the GNPs and IL, supplying good biocompatibility and high conductivity.

3.4. Amperometric response of the superoxide biosensor

For investigating the intrinsic biological catalytic activity of immobilized SOD, the response of SOD/GNP-CS-IL/GCE toward $O_2^{\bullet-}$ was measured by amperometric measurements (Fig. 5). A simple and efficient method for in situ generation of $O_2^{\bullet-}$ based on the xanthine/xanthine oxidase (XAN/XOD) system was employed in this work, which was described elsewhere and was confirmed by ESR [28]. It was reported that the combination of XAN 50–400 nM and XOD 0.002 U produced $O_2^{\bullet-}$ in a manner dependent on the concentration of XAN, and the yield of $O_2^{\bullet-}$ was 28% of the total XAN present in the reaction [6]. So, with successive additions of XAN to the solution, a stepwise increase of the current response was observed. The steady-state current was due to the simultaneous production and spontaneous dismutation of $O_2^{\bullet-}$ [29]. In detail, the generated $O_2^{\bullet-}$ could undergo automatic dismutation into O_2 and H_2O_2 under the experimental conditions. The counterbalance between the generation of $O_2^{\bullet-}$ and its degradation results in a constant equilibrium concentration of $O_2^{\bullet-}$ [22]. 95% of the steady-state current could be reached within 5 s. The rapidly decreased steady-state current at high concentrations of superoxide anion might be because hypoxanthine oxidation (superoxide production) had slowed down or finished. Moreover, the high concentration of superoxide anion might increase the chance of interactive collisions among the radicals, leading to the rapid decrease in the response. It was clear from the inset of Fig. 5 that SOD/GNP-CS-IL/GCE had an excellent linear response to $O_2^{\bullet-}$ in the concentration range from 5.6 to 2.7×10^3 nM, which was much wider than the 13–130 nM for a SOD-modified Au electrode [30]. A low detection limit of 1.7 nM (signal to noise (S/N) = 3) was obtained, which was not only evidently lower than the value of 15 nM for a SOD-PPr/Pt microelectrode [31], but also lower than the 100 nM detection limit for the ESR method [28]. From the above advantages, it can be seen that the present third-generation superoxide biosensor with nanomolar detection limits and a wide linear range meets the requirements for $O_2^{\bullet-}$ detection under normal physiological conditions (10^{-8}–10^{-7} M) [32].

3.5. Selectivity, reproducibility, and stability of the biosensors

It is well-known that coexisting biological compounds, such as H_2O_2, ascorbic acid (AA), and uric acid (UA), may cause difficulties for in vivo electrochemical determination of $O_2^{\bullet-}$ [33]. Hence, studying the influence of interfering species on the 1.1 μM $O_2^{\bullet-}$ monitor is of considerable importance. It was found that 10-fold H_2O_2 and UA, which were by-products in the XAN/XOD system to generate $O_2^{\bullet-}$, did not interfere with the tests for $O_2^{\bullet-}$. Moreover, the interference of a 1000-fold increase in AA was negligible in terms of $O_2^{\bullet-}$ detection.

The relative standard deviation (RSD) was 4.4% for 10 successive determinations of 1.1 μM $O_2^{\bullet-}$ using one single modified electrode. The result demonstrated excellent reproducibility of the biosensor for $O_2^{\bullet-}$ detection. The stability of the biosensor was also investigated. The biosensor could maintain 87% of its initial response after being stored for 44 days in a refrigerator. Owing to the above advantages, it can be inferred that the present biosensor is reliable for the measurement of $O_2^{\bullet-}$ in biological systems.

4. Conclusions

In this paper, GNP-CS-IL biocomposite film was prepared by a one-step ultrasonic electrodeposition method and was used to immobilize SOD to fabricate a new superoxide biosensor. The obtained SOD/GNP-CS-IL membrane possessed a uniform and smooth surface with a highly porous structure, and the entrapped SOD retained its native structure. The direct electron transfer between SOD and the underlying electrode was accelerated, suggesting the high conductivity and outstanding biocompatibility of GNPs and IL. In addition, these studies demonstrated that the biosensor had excellent analytical performance, such as wide linear range, a low detection limit on the nanomolar level, and high selectivity for quantitative $O_2^{\bullet-}$ detection. These results make clear that the present third-generation biosensor could be potentially useful for the physiological determination of $O_2^{\bullet-}$.

Acknowledgements

This work was supported by the National Natural Science Foundation of China (Nos. 20875023, 51173038), the Ph.D. Programs Foundation of the Ministry of Education of China (No. 20114208130001), the Natural Science Fund for Creative Research Groups of Hubei Province of China (No. 2011CDA111), and the Foundation for Innovative Research Groups of the Education Department of Hubei Province (No. T201101).

References

[1] F. Auchère, F. Rusnak, J. Biol. Inorg. Chem. 7 (2002) 664–667.
[2] Y. Tian, L. Mao, T. Okajima, T. Ohsaka, Biosens. Bioelectron. 21 (2005) 557–564.
[3] B. Halliwell, J.M.C. Gutteridge, Arch. Biochem. Biophys. 246 (1986) 501–514.
[4] R.P. Mason, K.T. Knecht, Methods Enzymol. 233 (1994) 112–117.
[5] S. Liu, J. Xing, Z. Zheng, F. Song, Z. Liu, S. Liu, Anal. Chim. Acta 715 (2012) 64–70.
[6] Y. Ohara, T.E. Peterson, D.G. Harrison, J. Clin. Invest. 91 (1993) 2546–2551.
[7] M.M. Tarpey, I. Fridovich, Circ. Res. 89 (2001) 224–236.
[8] C.J. McNeil, P. Manning, Rev. Mol. Biotechnol. 82 (2002) 443–455.
[9] Y.H. Bi, Z.L. Huang, Y.D. Zhao, Biosens. Bioelectron. 21 (2006) 1350–1354.
[10] L. Wang, W. Mao, D. Ni, J. Di, Y. Wu, Y. Tu, Electrochem. Commun. 10 (2008) 673–676.

[11] T. Tangkuaram, C. Ponchio, T. Kangkasomboon, P. Katikawong, W. Veerasai, Biosens. Bioelectron. 22 (2007) 2071–2078.
[12] V. Carralero Sanz, M. Luz Mena, A. Gonzalez-Cortes, P. Yanez-Sedeno, J.M. Pingarron, Anal. Chim. Acta 528 (2005) 1–8.
[13] K.S. Suslick, Encyclopaedia Britannica Yearbook of Science and the Future, Britannica, Chicago, 1994, pp. 138–155.
[14] S.C. Boca, M. Potara, F. Toderas, O. Stephan, P.L. Baldeck, S. Astilean, Mater. Sci. Eng. C 31 (2011) 184–189.
[15] M. Zhang, A. Smith, W. Gorski, Anal. Chem. 76 (2004) 5045–5050.
[16] X. Zeng, X. Li, L. Xing, X. Liu, S. Luo, W. Wei, B. Kong, Y. Li, Biosens. Bioelectron. 24 (2009) 2898–2903.
[17] J.S. Moulthrop, R.P. Swatloski, G. Moyna, R.D. Rogers, Chem. Commun. 12 (2005) 1557–1559.
[18] B.M. Quinn, Z. Ding, R. Moulton, A.J. Bard, Langmuir 18 (2002) 1734–1742.
[19] M. Yang, Y. Yang, H. Yang, G. Shen, R. Yu, Biomaterials 27 (2006) 246–255.
[20] F. Xiao, F.Q. Zhao, Y.F. Zhang, G.P. Guo, B.Z. Zeng, J. Phys. Chem. C 113 (2009) 849–855.
[21] H.J. Chen, S.J. Dong, Langmuir 23 (2007) 12503–12507.
[22] Y. Tian, L. Mao, T. Okajima, T. Ohsaka, Anal. Chem. 74 (2002) 2428–2432.
[23] S. Yang, W.Z. Jia, Q.Y. Qian, Y.G. Zhou, X.H. Xia, Anal. Chem. 81 (2009) 3478–3484.
[24] A.M. Bond, Modern Polarographic Methods in Analytical Chemistry, Marcel Dekker, New York, 1980.
[25] R.W. Murry, in: A.J. Bard (Ed.), Electroanalytical Chemistry, Marcel Dekker, New York, 1986, p. 191.
[26] M.S. El-Deab, T. Ohsaka, Electrochem. Commun. 9 (2007) 651–656.
[27] E. Laviron, J. Electroanal. Chem. 101 (1979) 19–28.
[28] H. Zhang, J. Joseph, J. Vasquez-Vivar, H. Karoui, C. Nsanzumuhire, P. Martasek, P. Tordo, B. Kalyanaraman, FEBS Lett. 473 (2000) 58–62.
[29] M.K. Beissenhirtz, F.W. Scheller, M.S. Viezzoli, F. Lisdat, Anal. Chem. 78 (2006) 928–935.
[30] T. Ohsaka, Y. Tian, M. Shioda, S. Kasahara, T. Okajima, Chem. Commun. 9 (2002) 990–991.
[31] S. Mesaros, Z. Vankova, A. Mesarosova, P. Tomcık, S. Grunfeld, Bioelectrochem. Bioenerg. 46 (1998) 33–37.
[32] Z. Deng, Q. Rui, X. Yin, H. Liu, Y. Tian, Anal. Chem. 80 (2008) 5839–5846.
[33] K.V. Gobi, F. Mizutani, J. Electroanal. Chem. 484 (2000) 172–181.